

VORONOI APPLIED ELEMENT METHOD FOR STRUCTURAL ANALYSIS: THEORY AND APPLICATION FOR LINEAR AND NON-LINEAR MATERIALS

K. Worakanchana¹ and K. Meguro²

¹ Project researcher, International Center for Urban Safety Engineering, Institute of Industrial Science, the University of Tokyo, Japan

² Director, International Center for Urban Safety Engineering, Institute of Industrial Science, the University of Tokyo, Japan
 Email: kawin@iis.u-tokyo.ac.jp

ABSTRACT :

Voronoi Applied Element Method (VAEM) has been developed based on previous Applied Element Method (AEM). Compared to the original AEM, the advantages of VAEM are: the VAEM domain boundary can fit any type of domain easily, pre-existing joint rather than horizontal and vertical joints can be modeled, element size can be changed and displacement solution is not depended on the element size and etc. The verification of the model from elastic to non-linear range is shown in the paper. The proposed model shows good compatibility with theoretical and experimental results.

KEYWORDS: Applied Element Method, Nonlinear analysis, Discrete element, Fractures, Failures

1. INTRODUCTION

Applied Element Method (AEM) is a numerical model for simulating structural behavior from elastic range to total collapse (Meguro and Tagel-Din, 1997). In AEM, a structure is modeled as an assembly of rigid elements connected together with zero-length normal and shear springs. The major advantages of AEM are simple modeling and programming and high accuracy of the results with relatively short CPU time. By using AEM, highly non-linear behavior, i.e. crack initiation, crack propagation, separation of the structural elements, rigid body motion of failed elements and totally collapse behavior of the structure can be followed with high accuracy. The model can achieve high accuracy in simulating behavior of those materials. However, due to the fact that the model contains only square shape element, there was several disadvantages. To eliminate these disadvantages, a new AEM based on Voronoi shape is proposed.

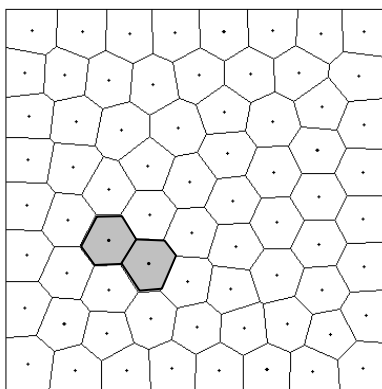


Figure 1 Example of a VAEM mesh

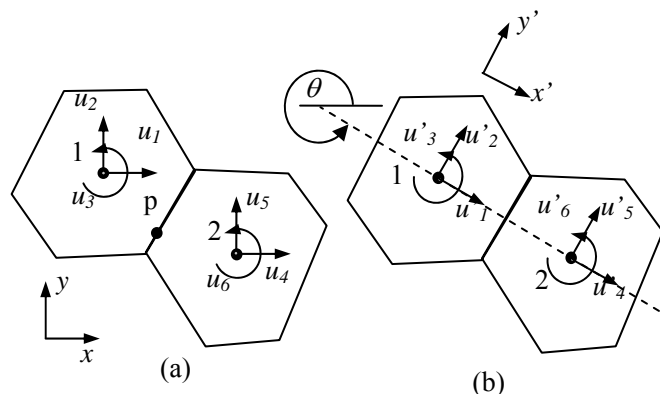


Figure 2 Two-particle assemblage and their degree of freedom (a) global coordinate (b) local coordinate

Each element shape is based on the Voronoi tessellation (Okabe et al., 1992). To represent the physical domain with the Voronoi element, first, element nodes are given in the space within the domain. Then, all locations in the physical domain are associated with the closest member(s) of the element nodal set with respect

to Euclidean distance. A region generated by a nodal point represents a Voronoi element (Figure 1).

Using the Voronoi Applied Element Method (VAEM), the element nodes can be placed anywhere in the physical domain with no constraint. Therefore, they can be placed to fit with any domain shape without considerably reducing the element size in the original AEM. Moreover, element sizes can be varied and concentrated in areas of interest by varying the density of element nodes. Also, the location of the element nodes can be placed to create weak zones representing pre-existing joints in any direction. In this paper, the formulation of the VAEM is introduced and verified in the elastic range and the non-linear range for reinforced concrete materials.

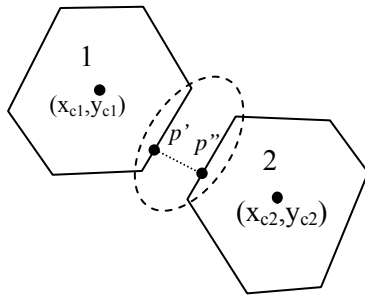


Figure 3 Two-particle assemblage after deformed

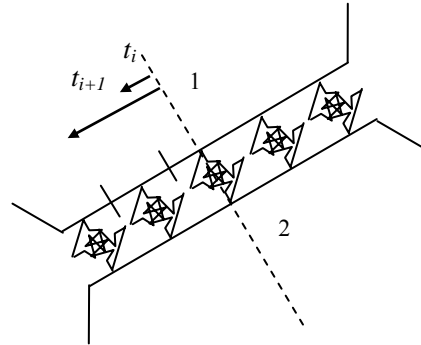


Figure 4 Normal and shear spring at element boundary

2. VORONOI APPLIED ELEMENT METHOD (VAEM)

2.1 Element Formulation

Considering a two-particle subassemblage shown in Figure 2, each rigid particle has two translational and a rotational degree of freedom defined at the particle centroid. Assuming small rotations, motion at any points (x, y) of a rigid body can be defined for element 1 and 2 as

$$\begin{aligned} u_1 &= u_{c1} - u_3(y - y_{c1}) & u_2 &= u_{c2} + u_3(x - x_{c1}) \\ u_4 &= u_{c4} - u_6(y - y_{c2}) & u_5 &= u_{c5} + u_6(x - x_{c2}) \end{aligned} \quad (1)$$

where u_1, u_2 and u_3 and u_4, u_5 and u_6 are translational displacements and rotation angles of elements 1 and 2 in the global coordinate. Subscript c specifies the value at the particle centroid. Point p on the boundary surface is separated and defined by p' and p'' after deforming (Figure 3). The relative displacement vector of spring deformation in global coordinate at point p can be defined as

$$\{\delta_g\} = \overrightarrow{p'p''} = \begin{Bmatrix} \delta_x \\ \delta_y \end{Bmatrix} = \begin{Bmatrix} u_4 - u_1 \\ u_5 - u_2 \end{Bmatrix} \quad (2)$$

Substituting Equation (1) into (2) and rotating the displacement to the local coordinate parallel to the element surface; we can obtain the relationship between spring deformation in local coordinate and particle displacement in global coordinate is obtained:

$$\{\delta\} = [\mathbf{R}][\mathbf{B}]\{u\} \quad (3)$$

where $\{\delta\}^T = [\delta_n, \delta_t]$ in which δ_n and δ_t are normal and shear deformation of spring, respectively, $[\mathbf{R}] = \begin{bmatrix} \cos \alpha & -\sin \alpha \\ \sin \alpha & \cos \alpha \end{bmatrix}$ is the rotational matrix, deformation-displacement relationship in global coordinates.

$[B] = \begin{bmatrix} -1 & 0 & (y-y_{c1}) & 1 & 0 & -(y-y_{c2}) \\ 0 & -1 & -(x-x_{c1}) & 0 & 1 & (x-x_{c2}) \end{bmatrix}$ and $\{u\}^T = [u_1, u_2, u_3, u_4, u_5, u_6]$. The strain energy due to spring deformation on the boundary line S can be given as

$$W = \frac{1}{2} \int \{\delta_i\}^T [D] \{\delta_i\} dS \quad (4)$$

where the constitutive relationship $[D] = \text{Diag}[k_{ni}, k_{si}]$ in which k_{ni} and k_{si} is stiffness of normal and shear springs number i , respectively. Applying Equation (8) into (9), we have:

$$W = \frac{1}{2} \{u\}^T [K] \{u\} \quad (5)$$

where $[K] = \sum_{i=1}^n \int_{t_i}^{t_{i+1}} [B]^T [D] [B] dS$ is the stiffness matrix due to all springs on the boundary. t_i and t_{i+1} indicate the initial and last points of the boundary portion representing the spring i (Figure 4). By applying Castigliano's theorem to Equation (5), stiffness equation can be derived as

$$\{r\} = \frac{\partial V}{\partial u} = [K] \{u\} \quad (6)$$

where $\{r\}$ contains the generalized force components associated with each displacement vector $\{u\}$.

2.2 Equivalent continuum

In this study, the relationship between discrete constants k_{ni} and k_{si} and the elastic properties follows the equivalent continuum method (Morikawa et.al., 1985). The method employs the equivalence of strain energy between the discrete and continuum system and the advantage of close-pack circular discrete element geometry. To apply this concept to the conventional AEM, it was found that these relationships are almost the same as the original proposed one but multiply by $\sqrt{3}$. Therefore, this relationship for VAEM is defined as

Plane stress:

$$k_{ni} = \frac{E \cdot t}{(1-\nu) \cdot d}, k_{si} = \frac{E \cdot t \cdot (1-3\nu)}{(1-\nu^2) \cdot d} \quad (7)$$

Plane strain:

$$k_{ni} = \frac{E \cdot t}{(1-2\nu)(1+\nu) \cdot d}, k_{si} = \frac{E \cdot t \cdot (1-4\nu)}{(1-2\nu)(1+\nu) \cdot d} \quad (8)$$

where E is elastic modulus, ν = Poisson's ratio, t = element thickness and d = distance between two particles. It should be noted that the Poisson's ratio is limited from -1 to 0.33 for plain stress and -1 to 0.25 for plain strain to prevent a negative value of tangential stiffness.

3. VERIFICATION FOR ELASTIC BEHAVIOR

In this section, the behavior of VAEM in elastic range is verified by analyzing a cantilever beam and a circular disk.

3.1 Cantilever beam

The cantilever beam with a cross-section of $1 \times 1 \text{ m}^2$ and 10 m span is subjected to the point load at the free end. Young's modulus is $2.14 \times 10^7 \text{ kN/m}^2$ and Poisson's ratio is 0. The displacement at the cantilever end obtained from VAEM and the original AEM are shown in the Table 1. The table shows that both square shaped and Voronoi shaped AEM results match well with the theoretical result.

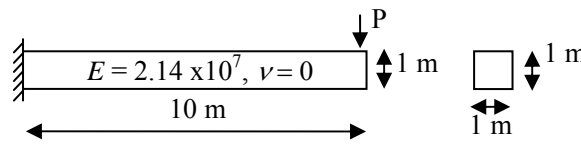


Figure 5 Geometry of cantilever beam

Table 1 Comparison of displacement at the cantilever end of VAEM, AEM and theoretical solution

	Exact ($PL^3/3EI$)	AEM	VAEM
δ_v (m)	9.20	9.12	9.22

3.2 Circular disk

This example shows the elastic analysis of a circular domain. This type of domain requires a large number of elements in the original AEM to obtain accurate results due to its single size square-shaped element. Figure 6 shows the VAEM mesh of circular disk of 8 unit diameter subjected to two point loads from the top and bottom of the disk. In this problem, the Young's modulus used is 2.14×10^7 . The stress distribution at the center line is compared with the theory of elasticity and good agreement is observed (Figure 7).

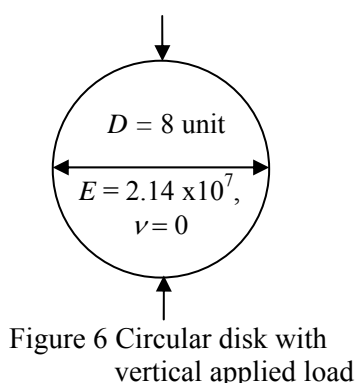


Figure 6 Circular disk with vertical applied load

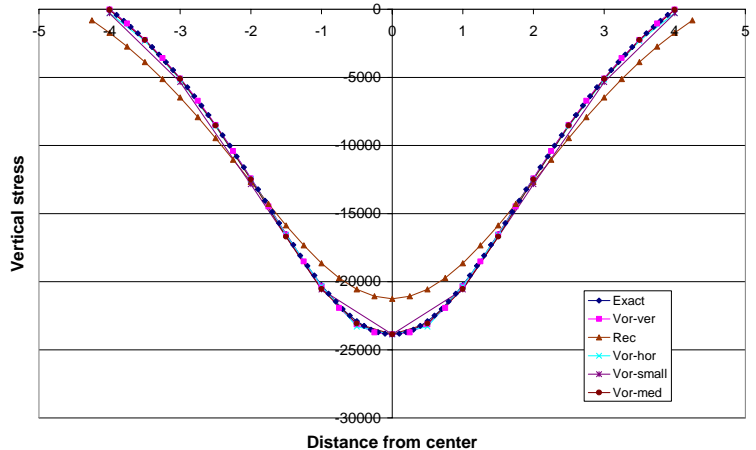


Figure 7 Comparison of stress distribution at the centerline from AEM, VAEM and exact solution

4. VAEM FOR FRACTURE ANALYSIS OF CONCRETE MATERIAL

The verification of VAEM for simulating plain and reinforced concrete structural behavior was conducted. The original AEM has capability of tracking the crack distribution without prior knowledge of the crack location. However, the crack distribution is limited to only the vertical and horizontal directions according to the element shape. With the VAEM, cracks have more freedom to propagate therefore the crack propagation can better follow the real crack patterns.

4.1 Concrete modeling

In this model, the behavior of the material is initially elastic, i.e., $\sigma = E\varepsilon$, where E is the apparent concrete Young's modulus. Inelastic behavior is formulated based on similar concept of stress-strain boundary introduced by Cusatis et al. (2003). Elastic behavior is limited by three boundaries, which are tension-shear, compression shear and compression as shown in Figure 8. This concept is based on the normal and shear stress in the springs rather than the tensorial measure of stress therefore the criteria can be biased based on the

mesh configuration. Schlangen (1995) used a criteria based on stress measures computed at the nodes of a beam lattice, rather than in the beams themselves. Moreover, Meguro and Hatem (1998) employed the principal stresses concept similar to the use of tensorial measure by Schlangen. However principal stresses is calculated at the springs themselves instead of element nodes. Employing the principal criteria approach is expected to reduce the mesh bias on the fracture criteria however it is not included in this study. In this model, a crack occurs if the force reaches tension-shear boundary. Cracking is represented by reducing the original to 0.01 of the initial stiffness. Then, all forces in normal and shear springs are redistributed. If the force reaches the compression shear and compression boundary, the stiffness of the spring is also assumed as 0.01 of the initial stiffness however no force is redistributed.

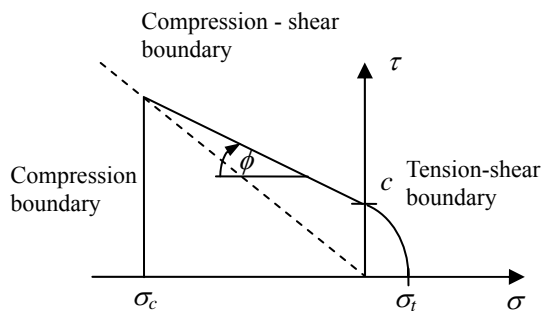


Figure 8 Stress-strain boundary for concrete

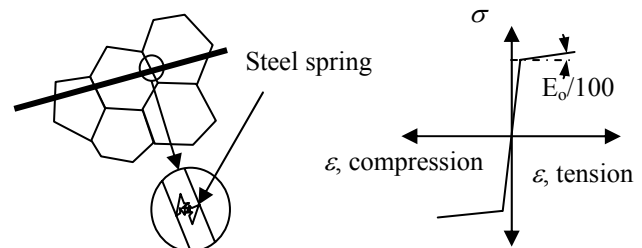


Figure 9 Steel springs and their material properties

4.2 Reinforcement model

Unlike the previous AEM, the normal and shear spring for reinforcement do not usually go along the edges of the elements. The reinforcement was modeled by adding the normal and shear springs inclined to edges as shown in Figure 9. In this study, perfectly plastic model was used in reinforcing bar to represent yielding (Figure 9).

4.3 Reinforced concrete modeling

In this section, VAMM is used to simulate the reinforced concrete behavior in the monotonic static loading condition. The numerical results are compared with the experiment results in the following sections.

Table 2 Material properties of concrete and steel of beams

Concrete		Steel			
F_{cu} (MPa)	F_t (MPa)	pr1	pr2	Diameter (mm)	Yield stress (MPa)
27.9	2.7	0.4%	0.8%	D16	362.8

4.4 Size effect analysis

A simulation of a beam from experiment by Iguro et al. (1985) was carried out. The beam was not provided with shear reinforcement. The material properties for beam are shown in Table 2. The beam dimensions, reinforcement as well as load-deformation behavior are shown in Figures 10. An applied load is uniformly distributed by water pressure system. The main reinforcement ratio “pr” in the vicinity of the supporting where shear failure would occur is taken to be 0.4% and it is taken to be 0.8% in the middle of the beam.

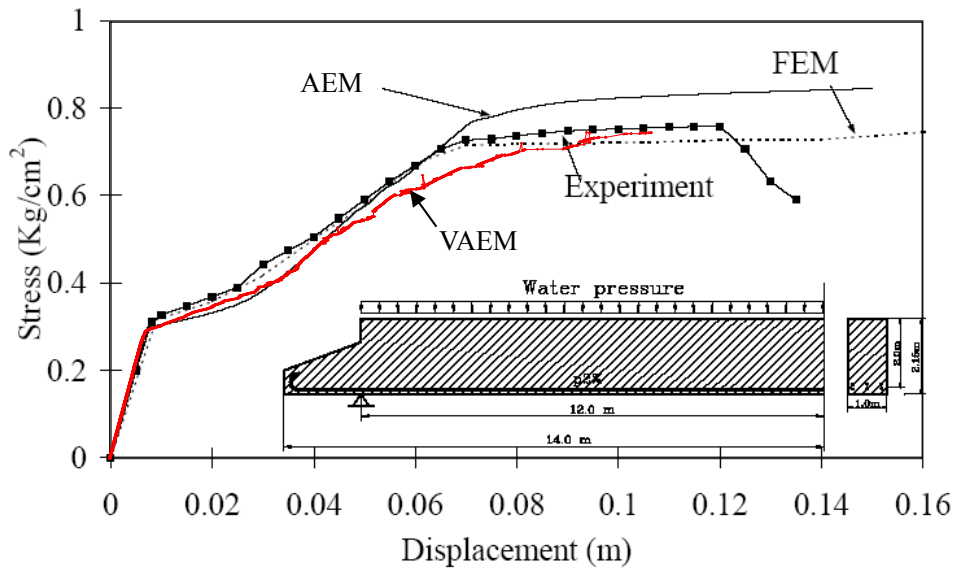


Figure 10 Comparison of stress-displacement relation

A mesh of 1,229 was used in the model. Loading is applied using load control condition. The comparison of the force-displacement relationship is shown in Figures 10. It can be seen that the force-deformation relationships obtained from VAEM are close to the experimental results and numerical results from AEM and FEM. However, VAEM exhibits lower strength compared to AEM because the diagonal crack in VAEM is represented by a shorter crack (less zigzag) which consumes less energy for generating. From Figures 11 to 13, by comparing crack patterns from VAEM with AEM and actual damage, it was observed that the crack patterns from VAEM is closer to the actual crack patterns than from AEM.

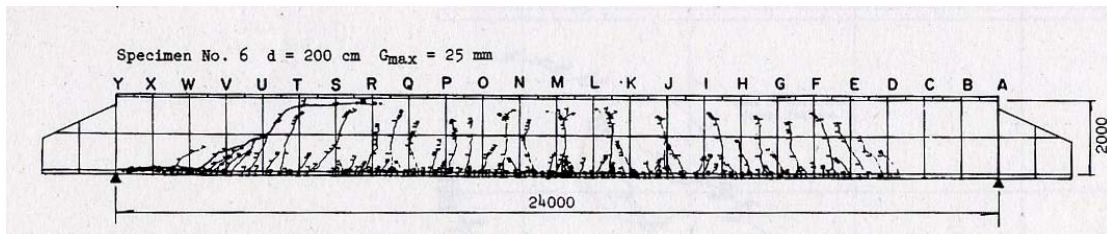


Figure 11 Crack pattern from experiment

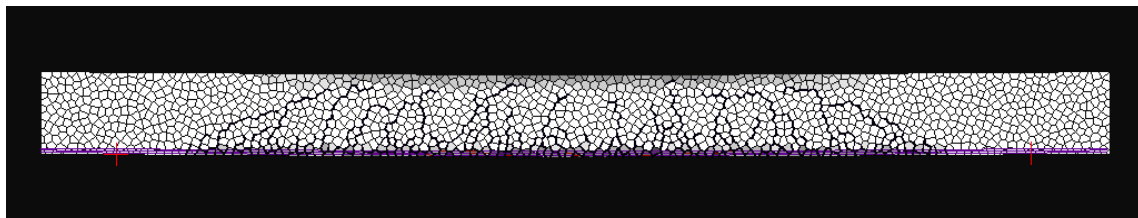


Figure 12 Crack patterns by VAEM

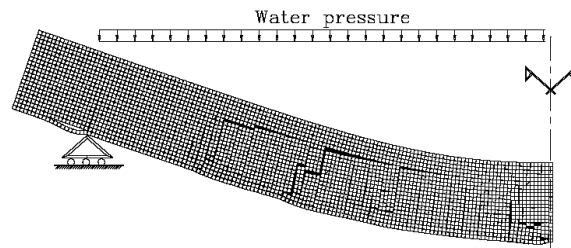


Figure 13 Crack pattern by the original AEM

5. LARGE DEFORMATION ANALYSIS

To simulate the structural behavior under large deformations, the geometrical change has to be considered during each step of the calculation. This requires the following additional procedures:

- 1) Update the location of the element node according to previously calculated incremental displacement
- 2) Calculate the geometrical residuals as

$$\{\mathbf{R}_G\} = \{\mathbf{f}\} - \{\mathbf{F}_m\} \quad (16)$$

This is to account for the incompatibility between the external applied forces vector, $\{\mathbf{f}\}$ and internal forces, $\{\mathbf{F}_m\}$ due to modification of geometry of the structure.

- 3) Take into account the geometrical residual in the stiffness equation which can be written as:

$$[\mathbf{K}]\{\mathbf{u}\} = \{\mathbf{r}\} + \{\mathbf{R}_G\} \quad (9)$$

The verification of this method is shown in the following paragraphs. The geometry of the beam subjected to the compressive load is shown in Figure 14. Young's modulus of the beam is equaled to 8.4×10^4 kN/m². The result obtained from the numerical model is compared with the analytical solution (Timoshenko, S.P. and Gere, J.M., 1961). The numerical model predicts closely values for the theoretical buckling load and force-displacement relationship of the post buckling behavior (Figure 15).

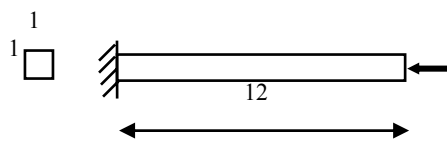


Figure 14 Beam geometry

6. CONCLUSIONS

The VAEM has been developed based on the original AEM. Elastic behavior of VAEM model was verified in this paper. Compared to the original AEM, the advantages of the VAEM are:

- The boundary, even very irregular one, domain is easier to fit.
- Pre-existing joints or weaker and/or stronger zones in any direction can be modeled.
- The model does not require numerical Poisson's ratio (however Poisson's ratio is limited from -1 to 0.33 in plain stress and -1 to 0.25 in plain strain).
- Varying the element size is simply done.
- Displacement solution is not depended of the element size

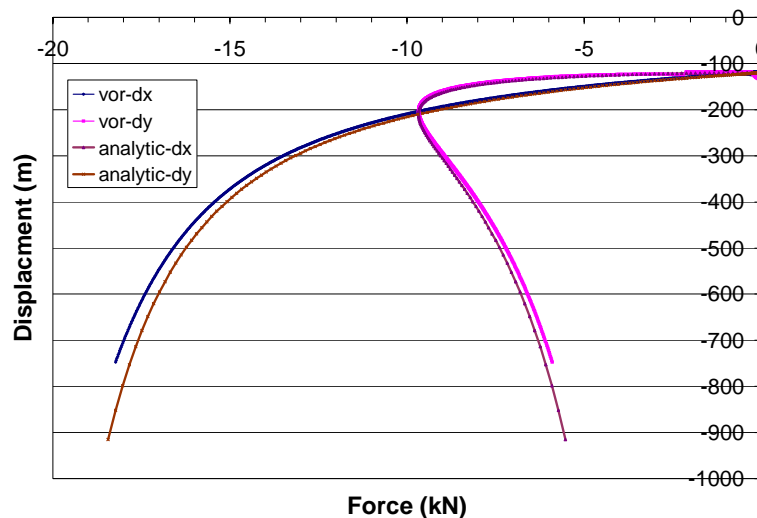


Figure 15 Comparison of the large deformation analysis from numerical model and analytic solution (vor-dx: x-direction displacement from Voronoi mesh; vor-dy: y-direction displacement from Voronoi mesh; analytic-dx: x-direction displacement from analytic result; analytic-dy: y-direction displacement from analytic result)

The VAEM was verified for predicting the behavior of plain and reinforced concrete. In all cases, the obtained crack locations agree well with the experimental results. In case of RC simulation, the diagonal crack obtained by VAEM was closer to experimental result than the original AEM because VAEM element boundary allows the crack to propagate closer to real crack. Moreover, because it consumes less energy to generate the shorter crack, VAEM result exhibits less maximum resistant compared to the AEM one.

REFERENCES

- Cusatis, G., Bazant Z. P., and Cedolin, L. (2003). Confinement-Shear Lattice Model for Concrete Damage in Tension and Compression: I. Theory. *J. Eng. Mech.*, 129: 12, 1439-1447.
- Iguro, M., Shioya, T., Nojiri, Y., and Akiyama, H. (1985). Experimental Studies on Shear Strength of Large Reinforced Concrete Beam under Distributed Load. *Concrete Library of JSCE*, 5, 137-154.
- Meguro, K., and Tagel-Din, H. (1997). Development and Application of New Model for Fracture Behavior Analysis of Structures. First US-Japan Workshop on Earthquake Engineering Frontiers in Transportation Facilities, Buffalo, New York, U.S.
- Morikawa, H., Sawamoto Y, and Kobayashi N. (1985) Local Fracture Analysis of a Reinforced Concrete Slab by Discrete Element Method. Proceeding of the 1st Conference on Numerical Methods and Fracture Mechanics, Swansea.
- Okabe, A., Boots, B., Sugihara K., and Nok Chiu, S. (1992). Spatial Tesselation Concepts and Applications of Voronoi Diagrams, 2nd ed., John Wiley & Sons, New York, U.S.
- Schlagen, E. (1995) Computational aspects of fracture simulations with lattice models. *Fracture Mechanics of Concrete structures*, Wittmann FH, Aedificatio, Freiburg, Germany, 913.
- Timoshenko, S.P. and Gere, J.M. (1961). Theory of elastic stability, 2nd Ed., McGraw-Hill, New York, U.S.